Supplementary Information

Lasing at multi-dimensional topological states in a two-dimensional photonic crystal structure

Authors

Changhyun Han[1,2], Minsu Kang[1,2], and Heonsu Jeon[1,2,3,*]

Affiliations

[1]Department of Physics and Astronomy, Seoul National University, Seoul 08826, Republic of Korea

[2]Inter-university Semiconductor Research Center, Seoul National University, Seoul 08826, Republic of Korea

[3]Institute of Applied Physics, Seoul National University, Seoul 08826, Republic of Korea

Calculation of the polarization as a topological invariant

In the theory of polarization in solids[1], the bulk dipole moment $\boldsymbol{p} = (p_x, p_y)$ of a 2D crystal is given by

$$p_{x,y} = -\frac{1}{(2\pi)^2}\int_{BZ} d^2\boldsymbol{k} Tr\left[i\langle u_m(\boldsymbol{k})|\partial k_{x,y}|u_n(\boldsymbol{k})\rangle\right],$$

where *m* and *n* represent the indices of all the bands below the band-gap of interest. We numerically calculate this value of our system by using a finite-difference time-domain (FDTD) software. Note that numerical evaluation of derivatives and integrations with respect to discrete k points relates this calculation to Wilson-loop approach, which has been introduced in previous studies[2-3]. It is also well-known that a mirror symmetry in $x(y)$ direction quantizes $p_x(p_y)$ to 0 or 0.5[2-3]. We first obtain eigenvectors $|u(k_x, k_y)\rangle$ by calculating the H_z field distribution in the unit cell at each discrete (k_x, k_y) point, and then numerically compute the bulk polarizations. Figure S1(a) shows the calculation results as a function of *d*. As expected, $p_x(p_y)$ shows a phase transition at $d = 0.25a$, where it jumps from 0 to 0.5, inferring that the 1D edge states can exist for $d > 0.25a$. Subsequently, the polarization of the edge state is calculated similarly from the bulk polarization for the topologically nontrivial domain $d/a > 0.25$. Calculation results are summarized in Fig. S1(b). It turns out that the edge states polarization is also nontrivial, which in turn guarantees the existence of the corner states.

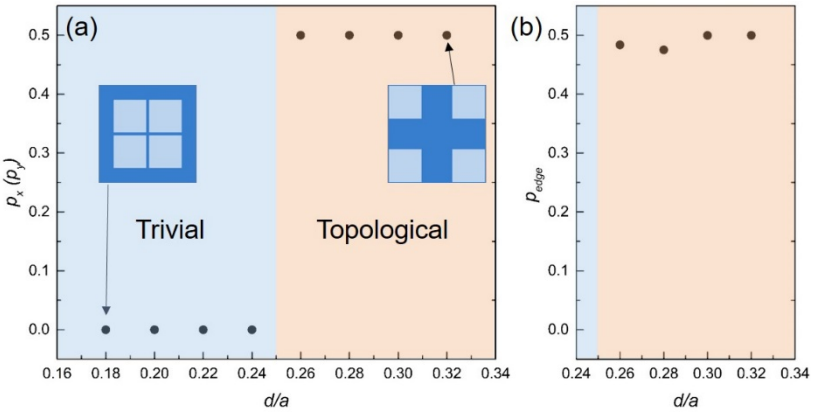

Fig. S1. Numerically calculated polarization. Polarization calculated as a function of *d/a* for (a) the bulk and (b) the edge.

Simulations on the ideal topological PhC structure

Although Figs. 3(c) and 3(d) in the main manuscript, which are simulation results on a realistic topological structure (with disorder), are more suitable to compare with the experimental results in Figs. 3(a) and 3(c), show all the salient features of the topological states in good agreement with the experimental results, it should be pedagogically correct to show simulation results on the ideal topological structure (without disorder). Shown below are modal spectra and profiles simulated for the ideal structure of the four-fold rotational symmetry. The four-fold rotational symmetry is clearly reflected in the simulated results on the edge and corner states.

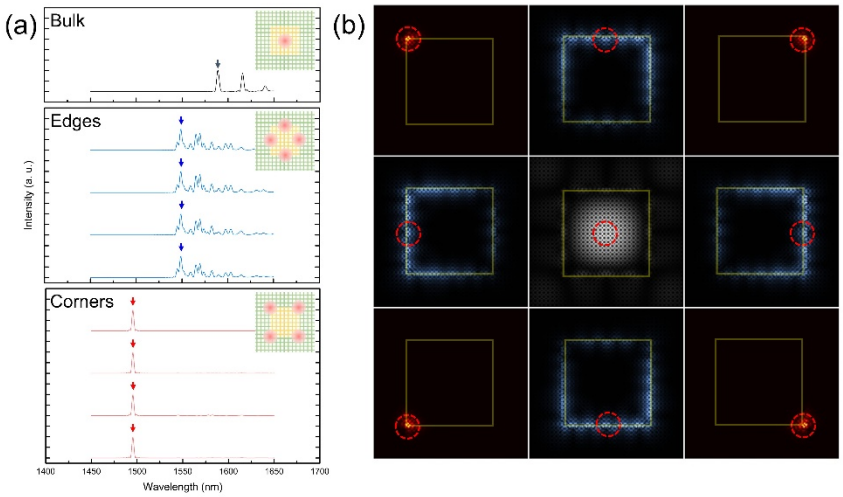

Fig. S2. Simulations on the ideal topological structure. (a) Simulated modal spectra of the bulk, edge, and corner states. (b) Simulated mode profiles of the bulk, edge, and corner states idicated by the arrows in (a).

Identification of the bulk states

An ideal band-edge laser structure should be infinitely periodic, although a real band-edge laser is always finite. When the excitation area is large enough to cover the entire laser structure, the device edges inevitably affect the formation of normal bulk modes and lift the modal degeneracy of the ideal band-edge laser, as already demonstrated by FDTD simulations in Fig. S2(a), which is copied here as Fig. S3(a). In order to prove that those three eigenmodes are indeed originated from a band-edge mode, we calculate their modal profiles, which are shown in Fig. S3(b). The shortest-wavelength mode (B1) resembles the ideal band-edge mode most, while the other two (B2 and B3) possess typical modal patterns of the higher-order modes within a square. For further assessment, we take Fourier-transformations of the modal profiles—Fig. S3(c). It is now inarguably clear that all the three modes are originated from the M-point band-edge mode.

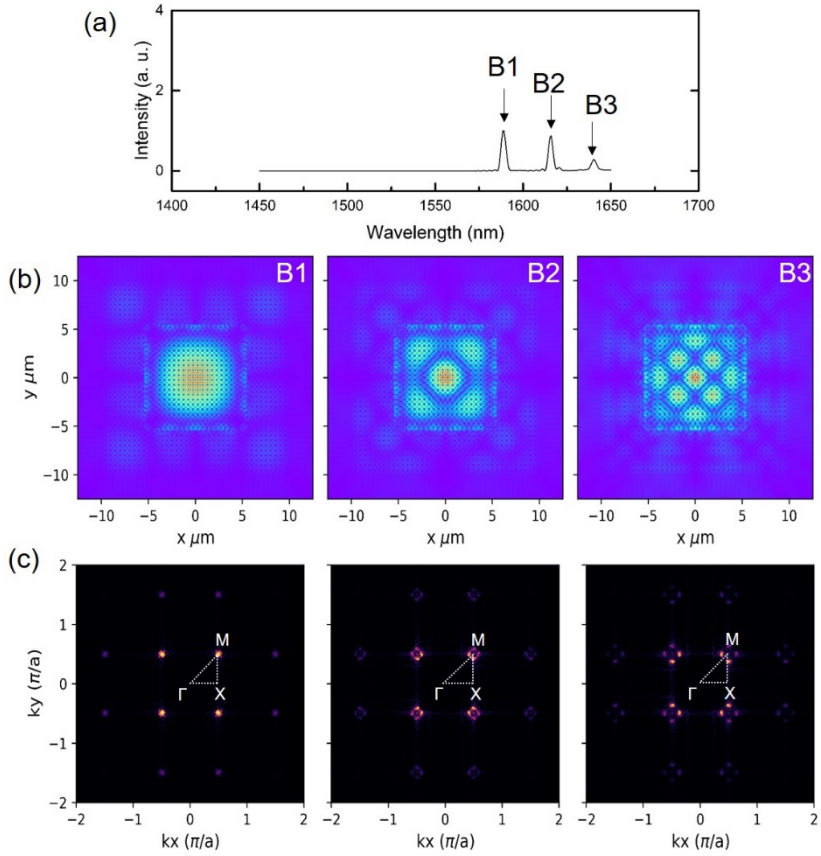

Fig. S3. Simulated bulk states. (a) FDTD-simulated modal spectra of the bulk states. (b) Mode profiles of the three bulk states identified in (a). (c) Fourier-transformation images of the three bulk mode profiles shown in (b). The irreducible Brillouin zone is inserted for reference.

Modal profiles of the edge states

In order to clarify the characteristics of the edge state lasers, we perform FDTD simulations. Figure S4(a) is the replot of the edge mode spectrum in Fig. S2(a), the simulated modal spectrum of the edge states in our topological PhC structure. Shown in Fig. S4(b) are the mode profiles of the three shortest-wavelength edge modes, which are identified by the arrows in Fig. S4(a). It should be noted that dipole sources are uniformed deployed along the four side edges this time, which differs from the situation for Fig. S2(b) where dipole sources are distributed only near the center of one side edge to mimic the optical excitation condition. One can see that the modal periodicity in each figure is commensurate with the underlying PhC lattice, which is modulated by an envelope function with a much longer period. We believe that the envelope function is a result of mode beating between multiple cavity lengths of L, $2L$, $3L$, and $4L$, where L is the side length of the square boundary.

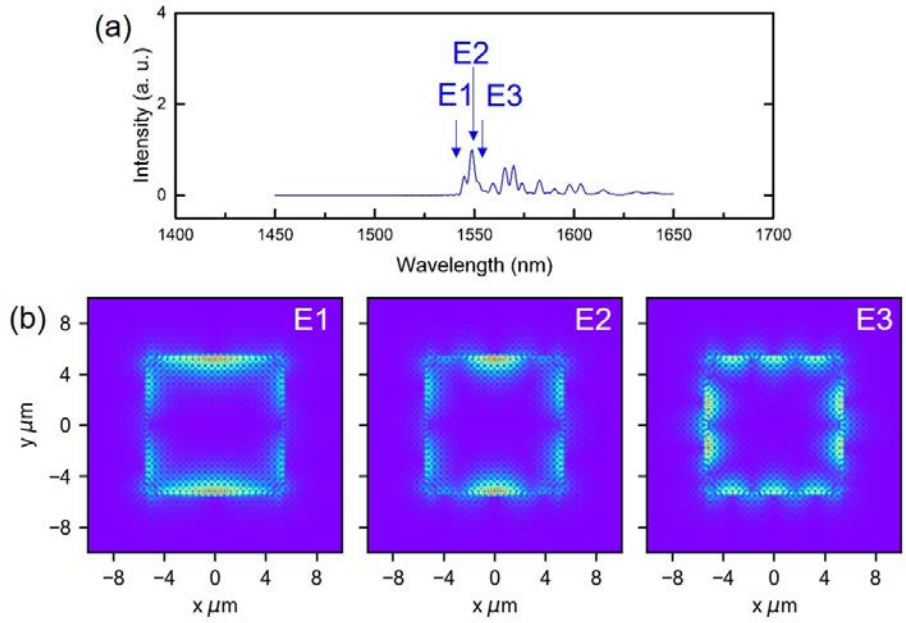

Fig. S4. Simulated edge states. (a) FDTD-simulated modal spectra of the edge states. (b) Simulated mode profiles of the three edge states of the shortest wavelengths, which are indicated by the arrows in (a).

Performance characteristics of the topological state lasers

To evaluate the qualities of the topological state lasers, light-in versus light-out characteristics were measured. Typical L-L curves for the nine different topological states, all measured from a single device, are shown in Fig. S5(a). Although the topological states are amply different, their lasing thresholds are rather similar, ~7 kW/cm^2. These experimental observations are qualitatively consistent with simulated results, which are summarized in Fig. S5(b): when a realistic topological structure (with disorder) is considered, simulated cavity Q-factors are in the order of 10^3 regardless of the topological states. The only exception is one edge state case where $Q \approx 10^4$, which we believe is because that particular area happens to contain less disorder.

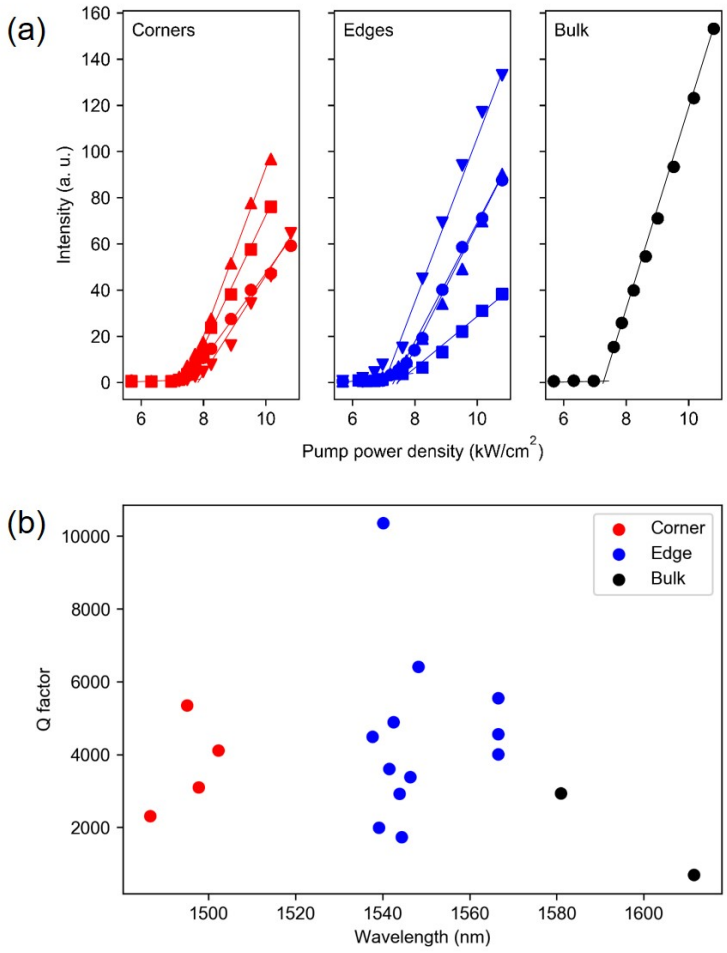

Fig. S5. Topological laser performance. (a) Relationships between light output intensity and excitation power density for the corner, edge, and bulk states. (b) Cavity Q factors calculated for the nine topological states present in a realistic model structure.

Modal robustness of the corner state

Modal robustness of the corner state has been investigated in a few previous studies[4-5]. In the present work, we examine an extreme situation where an edge defect, composed of a missing atom from a tetramer, is intentionally located very close to (or two lattices away from) a corner. Despite the existence of such a strong defect near the corner, the corresponding corner state is still well defined with the modal profile rarely disturbed, as can be seen in Fig. S6. The calculated Q-factors are ~3,100 and ~2,500 without and with the defect, respectively.

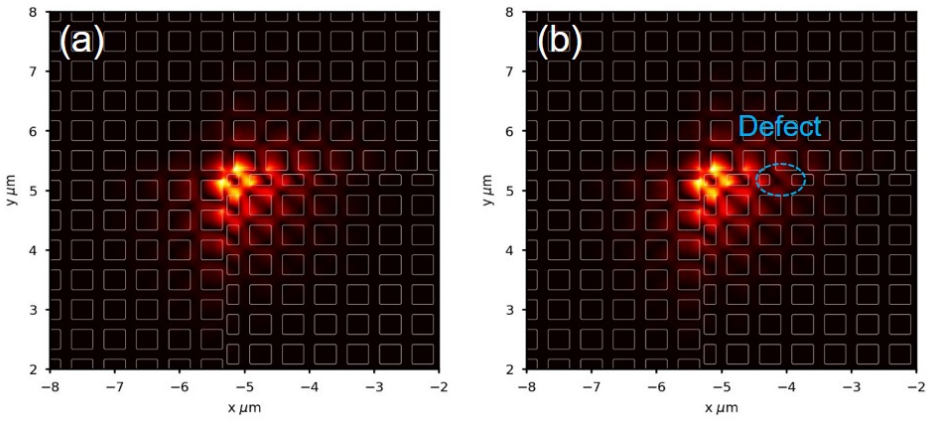

Fig. S6. Robustness of the corner state. (a)(b) Simulated electric field profiles of the corner states (a) without and (b) with a defect.

Stable single-mode nature of the corner state

The number of TESs is protected by the bulk-edge correspondence. This is a very powerful and desirable characteristic for single-mode laser operation[6-7], because even a small-size PhC cavity may support multiple modes originated from higher-order modes or different polarizations. We compare our topological corner cavity with the celebrated PhC L3 cavity via simulations. Figure S7(a) shows a simulated spectrum of the L3 cavity (lattice period a = 450 nm; air-hole radius r = 0.3a; slab thickness t = 230 nm). Despite the small size, the L3 cavity supports several modes; the corresponding modal profiles are shown in Fig. S7(b). On the contrary, the corner state remains single mode as long as the band-gap is present. Figure S7(c) shows a simulated spectral map, which exhibits the evolutions of the bands (green), band-gaps (black), and corner state (yellow) as a function of Δ; the spectra are presented in logarithmic scale for clear identification of the band-gaps. It is clear that there is only one corner state mode inside the main band-gap until the gap closes at $\Delta \sim 0.05a$. Figure S7(d) shows the mode profiles of the corner state for four different Δ's, demonstrating that a tightly-confined (therefore stable) corner state is well preserved until the band-gap collapses and the corner state is hybridized with the bulk or edge states.

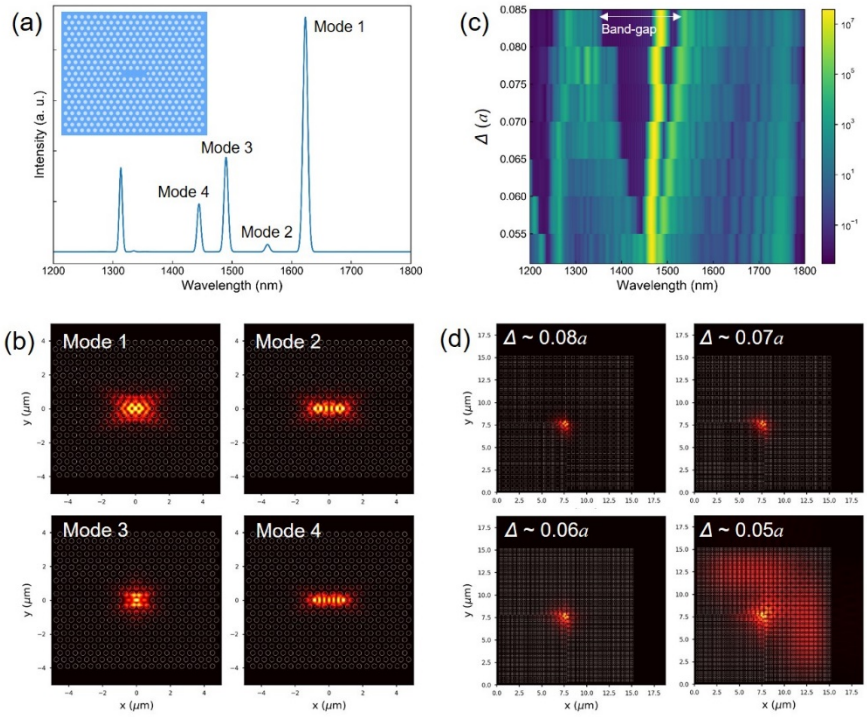

Fig. S7. Stability of the corner state. (a) Simulated modal spectrum of the PhC L3 cavity. (b) Modal profiles of the four low frequency modes in (a). (c) Simulated spectral map obtained near the corner of the topological PhC structure. A single corner mode exists in the photonic band-gap, which is indicated by an arrow. (d) Modal profiles of the corner states at different Δ values.

Supplementary References

(1) King-Smith, R. D.; Vanderbilt, D., Theory of polarization of crystalline solids. *Phys. Rev. B* **1993,** *47* (3), 1651-1654.
(2) Benalcazar, W. A.; Bernevig, B. A.; Hughes, T. L., Quantized electric multipole insulators. *Science* **2017,** *357* (6346), 61-66.
(3) Benalcazar, W. A.; Bernevig, B. A.; Hughes, T. L., Electric multipole moments, topological multipole moment pumping, and chiral hinge states in crystalline insulators. *Phys. Rev. B* **2017,** *96* (24), 245115.
(4) Xie, B.-Y.; Wang, H.-F.; Wang, H.-X.; Zhu, X.-Y.; Jiang, J.-H.; Lu, M.-H.; Chen, Y.-F., Second-order photonic topological insulator with corner states. *Phys. Rev. B* **2018,** *98* (20), 205147.
(5) Chen, X.-D.; Deng, W.-M.; Shi, F.-L.; Zhao, F.-L.; Chen, M.; Dong, J.-W., Direct Observation of Corner States in Second-Order Topological Photonic Crystal Slabs. *Phys. Rev. Lett.* **2019,** *122* (23), 233902.
(6) Ota, Y.; Katsumi, R.; Watanabe, K.; Iwamoto, S.; Arakawa, Y., Topological photonic crystal nanocavity laser. *Communications Physics* **2018,** *1* (1), 86.
(7) Han, C.; Lee, M.; Callard, S.; Seassal, C.; Jeon, H., Lasing at topological edge states in a photonic crystal L3 nanocavity dimer array. *Light: Science & Applications* **2019,** *8* (1), 40.